Catalyst-free low temperature conversion of *n*-dodecane for co-generation of CO_x-free hydrogen and C_2 hydrocarbons using a gliding arc plasma

Yichen Ma, Jonathan D. Harding, Xin Tu*

Department of Electrical Engineering and Electronics, University of Liverpool, Liverpool, L69 3GJ, UK

*Corresponding Author (Dr. Xin Tu)

E-mail: xin.tu@liv.ac.uk

Abstract

In this study, plasma reforming of *n*-dodecane for the co-generation of CO_x-free hydrogen and C_2 hydrocarbons at low temperatures and ambient pressure has been investigated in a gliding arc discharge (GAD) reactor. The selective synthesis of H_2, C_2H_2 and C_2H_4 and the energy efficiency for *n*-dodecane conversion can be tuned by changing different processing parameters including gas flow rate, *n*-dodecane concentration and input voltage. The highest selectivity of H_2 (76.7%), C_2H_2 (41.4%) and C_2H_4 (12.0%) was achieved at *n*-dodecane conversion 68.1%. The generation of mixed hydrogen, acetylene and ethylene offers the possibility for in-situ hydrogenation to enhance the selectivity of light olefins (e.g., ethylene) without prior gas separation. The plausible reaction mechanism and pathways in the plasma cracking of *n*-dodecane have been discussed through plasma emission spectroscopic diagnostics coupled with a comprehensive analysis of gas and liquid products. A strong correlation between the yield of C_2 hydrocarbons and the relative intensity of C_2 Swan bands was found, which suggests that C_2 Swan bands could be used as a valuable probe to understand the generation of C_2 hydrocarbons in the plasma reforming of hydrocarbons oils.

Keywords: Non-thermal plasma; *n*-Dodecane; Hydrocarbon oils; Hydrogen production; C_2 hydrocarbons

1. Introduction

Converting heavy hydrocarbons, especially waste hydrocarbon oils to valuable fuels and chemicals has attracted increasing interest in the past years. One example is on-board hydrogen generation from liquid hydrocarbons for fuel cell powered auxiliary power units (APUs) in transportation, which can avoid the additional costs related to hydrogen storage and distribution [1-6]. On-site hydrogen generation from liquid hydrocarbons is also attractive to the chemical industry, in particular for any chemical synthesis that uses hydrogen as a feedstock such as hydrogenation [7-10]. In the petrochemical and refinery industry, heavy hydrocarbons are important sources for the synthesis of light olefins via thermal cracking or fluid catalytic cracking (FCC) at high temperatures [11-13].

However, conventional thermal processing of heavy hydrocarbons for the production of hydrogen or olefins is energy intensive as these processes are usually operated at high temperature and/or high pressure. Catalysts are often used in these processes to improve the selectivity of target products. However, catalyst deactivation due to carbon deposition while processing of heavy hydrocarbons remains a major challenge [14-16]. For example, in the fluid catalytic cracking process periodical catalyst regeneration in air at high temperatures (e.g., 800 °C) is required to burn off the deposited coke, incurring additional energy consumption.

Non-thermal plasma (NTP) technology is considered an unconventional but promising process for the synthesis of valuable fuels and chemicals from a variety of carbon sources (e.g., CH_4 and CO_2) using low temperatures and ambient pressure [17-19]. Free electrons initially formed in NTP can react with background gases and feed reactants to produce a cascade of reactive species including free radicals and excited species which are not available in conventional thermal or catalytic processes, therefore creating new reaction routes for chemical synthesis. Although the electrons have very high temperatures, the temperature of the heavy particles is far lower, and thus, the gas can be close to room temperature [20-22]. Such a non-equilibrium advantage of NTP is unique and enables thermodynamically unfavourable chemical reactions (e.g., hydrocarbon reforming) to proceed at low temperatures. Non-thermal plasma processes for chemical synthesis can be switched on and off instantly and can be integrated with renewable energy (e.g., wind or solar power) to reduce the energy costs for mobile or distributed systems for chemical energy storage.

Although significant efforts using different plasma systems have been dedicated to the activation of methane and liquid alcohol fuels (e.g., methanol and ethanol) [23-26]; far less has been done in regards to the application of non-thermal plasmas on hydrocarbon oils such as *n*-dodecane, a major component of diesel and kerosene and a typical waste organic solvent from nuclear industry, which could be converted into valuable fuels and chemicals, including hydrogen and light hydrocarbons [27-33]. Prantsidou and Whitehead investigated the degradation of gas phase *n*-dodecane at a

low concentration (65 ppm) in a dielectric barrier discharge (DBD) system packed with $BaTiO_3$ using N_2 and N_2/O_2 as the carrier gas. The formation of NO_x was found due to the presence of N_2 and O_2 in the plasma process [27]. They also evaluated the effect of carrier gas (Ar and N_2) and gas humidity on the conversion of liquid phase *n*-dodecane using a gliding arc discharge (GAD) via both batch and recirculating treatments. In addition to the production of CH_4, C_2H_2 and C_2H_4, CO and CO_2 were also detected in the plasma processing of *n*-dodecane using Ar/H_2O, while HCN and NO were found when using N_2/H_2O [28]. Zhang and Cha developed an aqueous discharge reactor that uses gaseous bubbles (Ar, Ar/CH_4 and Ar/CO_2) for the conversion of *n*-dodecane mixed with water into synthetic liquid fuels and syngas [29]. A GAD reactor with a reverse vortex flow was developed for the reforming of liquid *n*-dodecane to hydrogen-rich syngas (mainly CO and H_2) with limited yields of C_2 hydrocarbons [30]. Clearly, limited efforts have been concentrated on the use of non-thermal plasmas for the transformation of *n*-dodecane into valuable fuels and chemicals while minimizing the production of unwanted by-products, especially NO_x and CO_2. It is of crucial importance to better understand how different operating parameters affect the plasma conversion of *n*-dodecane and how to tune the process (e.g., *n*-dodecane conversion, energy efficiency and gas yield) by choosing appropriate processing parameters. In addition, the plasma chemistry and reaction mechanisms involved in the NTP processing of *n*-dodecane are still not clear. Therefore, gaining better insights into the reaction pathways in the NTP cracking of *n*-dodecane through a combined means of chemical analysis and plasma diagnostics

could generate essential and invaluable knowledge for the future development of this attractive and emerging technology.

In this study, we report a catalyst-free, low-temperature process for the co-generation of CO_x-free hydrogen and C_2 hydrocarbons at ambient pressure via the plasma cracking of *n*-dodecane using a bench-scale GAD reactor. Compared to other types of NTP such as corona discharge and DBD, gliding arc has been shown to be more effective for the conversion of carbon-based molecules, especially large carbon molecules due to its significantly higher electron density. The influence of *n*-dodecane concentration, total flow rate and applied voltage on the conversion of *n*-dodecane in the humid nitrogen GAD have been assessed in terms of the conversion of *n*-dodecane, the yield/selectivity of hydrogen and C_2 hydrocarbons and the process efficiency. Optical emission spectroscopic (OES) diagnostics were employed to investigate the generation of reactive species and their roles in the distribution of gaseous products. A plausible reaction mechanism in the plasma cracking of *n*-dodecane has been discussed in detail.

2. Experimental

2.1 Experimental setup

Figure 1 presents a schematic of the reaction system. In this work, the experiment was carried out in a traditional GAD system operated at low temperature and atmospheric pressure. Two diverging stainless-steel electrodes (60 mm in length, 18 mm in width)

were installed 3 mm downstream of the nozzle exit with a minimum discharge gap of 2 mm. The plasma system was powered by an AC high voltage neon transformer with a maximum peak-to-peak voltage of 10 kV and a fixed frequency of 50 Hz. A high voltage probe (Testec, TT-HVP 15 HF) was used to measure the arc voltage, while a current transformer (Magnelab CT) was used to monitor the arc current. Both electrical signals were recorded by a Tektronix digital oscilloscope (DPO2024B). The typical arc voltage and arc current of the N_2/*n*-$C_{12}H_{26}$/H_2O GAD are plotted in Figure S1 in the Supporting Information. The temperature of the gliding arc at 50 mm downstream of the nozzle exit was 90-110 ˚C, measured by an Omega fibre optical temperature probe (FOB102).

The flows of deionized water and *n*-dodecane (*n*-$C_{12}H_{26}$, Reagent Plus >= 99%) were controlled by high-precision syringe pumps (KDS Legato, 100), with nitrogen (BOC, zero grade, 99.999% purity) as a carrier gas. A mixed stream of 20 ml *n*-dodecane, 20 ml deionized water and nitrogen was preheated at 250 ˚C in a tube furnace (Carbolite, MTF12/38/250) to produce a steady stream of vapour which was injected into the GAD system. The concentration of *n*-dodecane in this study varied from 468 to 1400 ppm, while the steam/carbon (S/C) molar ratio was kept low at 0.25 to limit carbon deposition and CO_2 formation.

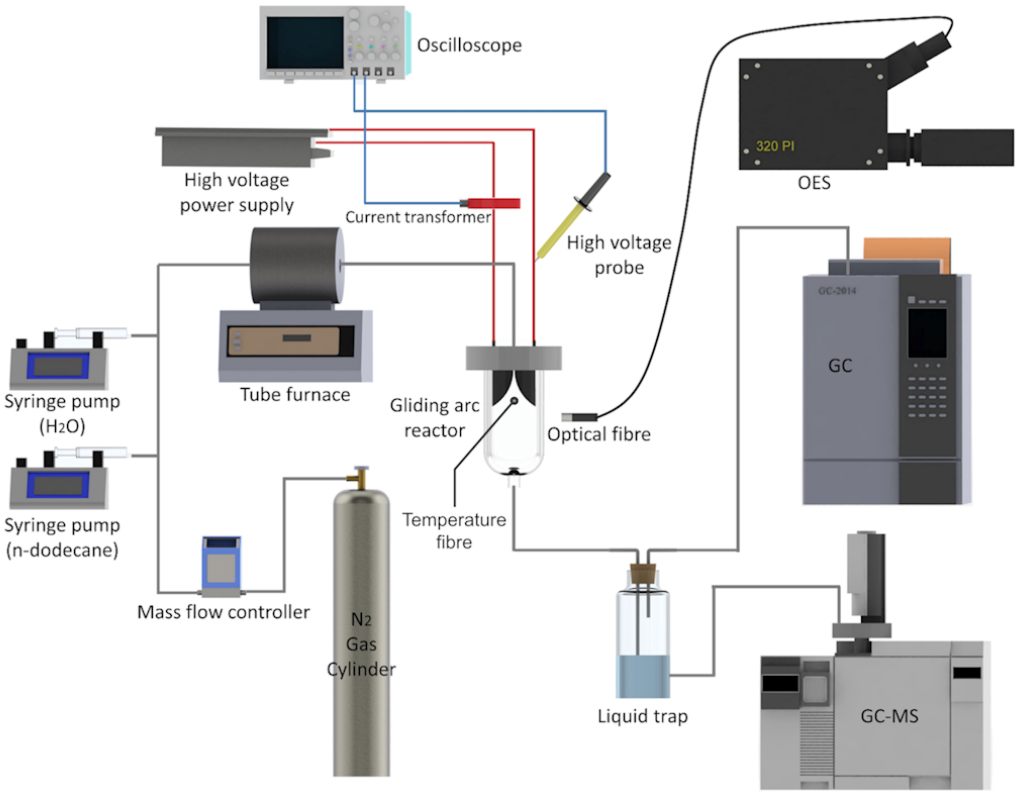

Figure 1. A schematic of the experimental system

2.2 Product analysis

Condensable products were collected in a flask placed in an ice-water mixture and dissolved in 200 ml of methanol (Fisher Chemical, Extra Pure). Gas chromatography-mass spectrometry (GC/MS, Agilent GC 7820A and Agilent MSD 5975C) was used to measure the liquid products, which were qualitatively analysed using a database from the National Institutes for Standards and Technology (NIST). Gaseous products were measured by a Shimadzu two-channel gas chromatograph (GC-2014) with dual detectors (thermal conductivity detector and flame ionization detector). The first channel consisted of a Molecular Sieve 5A (60-80 mesh) column for the separation of H_2 and CO, while the second channel was equipped with a HayeSep N (60-80 mesh) column for the measurement of CO_2, CH_4 and C_2-C_4

hydrocarbons. The emission spectra (200-900 nm) from the GAD was measured by a spectrometer (Princeton Instruments, 320PI) with an ICCD camera. An optical fibre connected to the spectrometer was positioned on the central axis of the electrode gap within the arc ignition zone, 25 mm downstream of the nozzle exit.

The discharge power of the gliding arc is determined through the integral of arc voltage multiplied by arc current:

$$P(\mathrm{W}) = \frac{1}{\mathrm{T}}\int_0^{t=\mathrm{T}} U(t)\times I(t)\mathrm{d}t \tag{1}$$

The conversion of *n*-dodecane ($X_{n\text{-}C_{12}H_{26}}$) can be defined as:

$$X_{n\text{-}C_{12}H_{26}}\,(\%) = \frac{\text{moles of } n\text{-}C_{12}H_{26} \text{ converted}}{\text{moles of } n\text{-}C_{12}H_{26} \text{ input}} \times 100 \tag{2}$$

The yield of gaseous products can be determined as:

$$Y_{H_2}\,(\%) = \frac{2\times \text{moles of } H_2 \text{ produced}}{26\times \text{moles of } n\text{-}C_{12}H_{26} \text{ input} + 2\times \text{moles of } H_2O \text{ input}} \times 100 \tag{3}$$

$$Y_{C_xH_y}\,(\%) = \frac{x\times \text{moles of } C_xH_y \text{ produced}}{12\times \text{moles of } n\text{-}C_{12}H_{26} \text{ input}} \times 100 \tag{4}$$

The selectivity of gaseous products is defined as follows:

$$S_{H_2}\,(\%) = \frac{Y_{H_2}}{X_{n\text{-}C_{12}H_{26}}} \tag{5}$$

$$S_{C_xH_y}\,(\%) = \frac{Y_{C_xH_y}}{X_{n\text{-}C_{12}H_{26}}} \tag{6}$$

The specific energy input (*SEI*) is given by Eq. (7).

$$SEI\ (\mathrm{kWh/m^3}) = \frac{P(\mathrm{kW})}{\text{Total flow rate } (\mathrm{m^3/h})} \tag{7}$$

The energy efficiency of *n*-dodecane conversion (η_e) and the hydrogen production efficiency (η_{H2}) of the plasma process are defined as:

$$\eta_e \text{ (g/kWh)} = \frac{\text{converted } n\text{-}C_{12}H_{26}\,(\text{g/m}^3)}{SEI\ (\text{kWh/m}^3)} \tag{8}$$

$$\eta_{H_2} \text{ (g/kWh)} = \frac{\text{produced } H_2\,(\text{g/m}^3)}{SEI\ (\text{kWh/m}^3)} \tag{9}$$

2.3 Calculation of bond-dissociation energy

To gain new insight into the reaction mechanism in the plasma conversion of *n*-dodecane, bond-dissociation energies (BDEs) were calculated at different positions of the *n*-dodecane molecule using density functional theory (DFT) with Spartan software. The geometry optimization of the *n*-dodecane molecule was carried out at the B3LYP/6-311+G** level of theory, which is generally considered reliable and computationally efficient. The homolytic C-H bond-dissociation energies of *n*-dodecane in this work were estimated from the expression:

$$C_x\text{-}H \rightarrow C_x^{\bullet} + H^{\bullet} \tag{10}$$

in which $C_x\text{-}H$ represents parent *n*-dodecane molecules; $C_x^{\bullet}$ is equal to dodecyl radicals, and $H^{\bullet}$ signifies hydrogen atoms. The BDEs were calculated by the following equation:

$$\text{BDE} = \Delta_f H(C_x^{\bullet}) + \Delta_f H(H^{\bullet}) - \Delta_f H(C_x\text{-}H) \tag{11}$$

in which $\Delta_f H(i)$ is the standard enthalpy of formation for the species *i* at 298.15 K.

3. Results and discussion

3.1 Influence of *n*-dodecane concentration

The influence of the *n*-dodecane concentration on the conversion and energy efficiency is illustrated in Figure 2(a). The conversion of *n*-dodecane declined from 79.4% to 69.2% when increasing the concentration at a fixed plasma power, which can be attributed to a decrease in the power density per molecule of *n*-dodecane. There is a trade-off between energy efficiency and *n*-dodecane conversion, as with a higher *n*-$C_{12}H_{26}$ concentration the total amount of converted *n*-$C_{12}H_{26}$ molecules increased despite the decreasing conversion, leading to a lower energy cost.

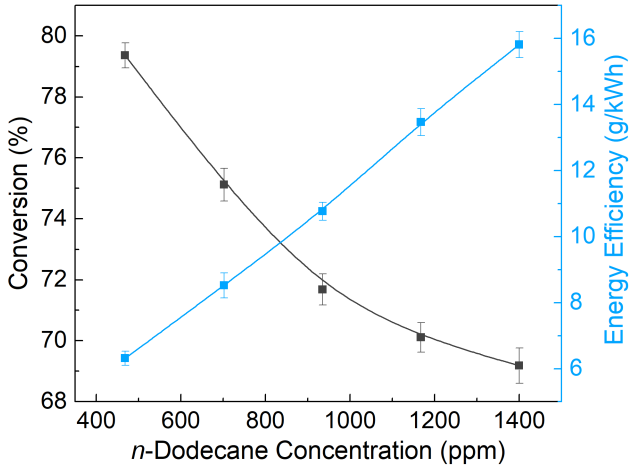

(a)

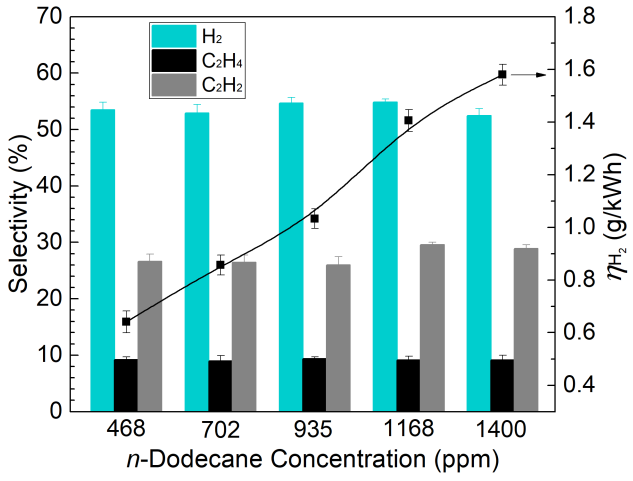

(b)

Figure 2. The influence of *n*-dodecane concentration on (a) the conversion of *n*-dodecane and energy efficiency; (b) the selectivity of major gas products and hydrogen production efficiency (total flow rate 3.5 L/min; plasma power 110 W).

The gaseous products identified in this reaction included H_2 and hydrocarbons (CH_4, C_2H_2, C_2H_4, C_2H_6, and C_3H_8) with H_2, C_2H_2, and C_2H_4 being the most dominant. Figure 2(b) shows that the selectivity of these major gaseous products remained stable, with only minor fluctuations when increasing the *n*-dodecane concentration. Compared to other operating parameters such as discharge power, total flow rate and residence time, changing the reactant concentration does not significantly affect the reaction pathways, leading to very little change in the gas selectivity as a function of *n*-dodecane concentration (Figure 2(b)). Similar findings were also reported in previous studies on the plasma dry reforming of methane [34]. H_2 was produced as the most abundant gas product with the highest selectivity of 54.9%, followed by C_2H_2 (up to 28.9% selectivity) and C_2H_4 (around 9.2%). The production of a high percentage of hydrogen in this reaction coincided well with a previous study on GAD reforming for the production of hydrogen-rich gas [30]. The total selectivity of minor gaseous products was approximately 5.0%. In addition, the energy efficiency of hydrogen production increased almost linearly with the increase of the concentration of *n*-dodecane. This phenomenon can be attributed to the increased amount of

converted *n*-$C_{12}H_{26}$ and enhanced hydrogen production when increasing the *n*-dodecane concentration.

3.2 Influence of total flow rate

Figure 3(a) shows the influences of the N_2 flow rate on the conversion of *n*-dodecane, the converted amount of *n*-dodecane and the energy efficiency. Below 2.75 L/min, a continuous arc was unable to be self-sustained in this reactor. The conversion of *n*-dodecane decreased from 77.3% to 68.1% when increasing the flow rate from 2.75 to 3.75 L/min. Increasing nitrogen flow rate decreased the residence time in the plasma area thus reducing the chance of *n*-dodecane and its fragments reacting with the chemically reactive species such as energetic electrons and radicals in the plasma reaction [35]. However, as shown in Figure 3(a), the lower flow rate could limit the total number of *n*-$C_{12}H_{26}$ molecules passing through the plasma zone, thus reducing the amount of converted *n*-dodecane. These findings indicate that a high total flow rate is favourable from the perspective of energy efficiency. It can be seen that the energy efficiency for conversion increased almost linearly from 9.2 to 10.9 g/kWh when increasing nitrogen flow, correlating well with the converted amount of *n*-$C_{12}H_{26}$ as a function of total N_2 flow rate.

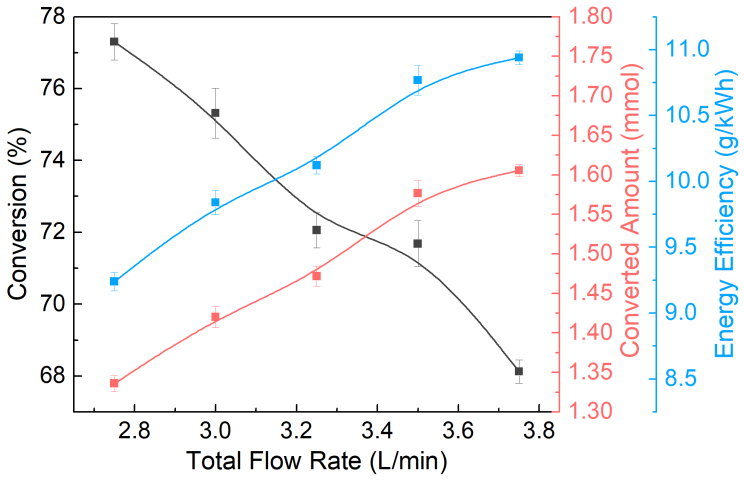

(a)

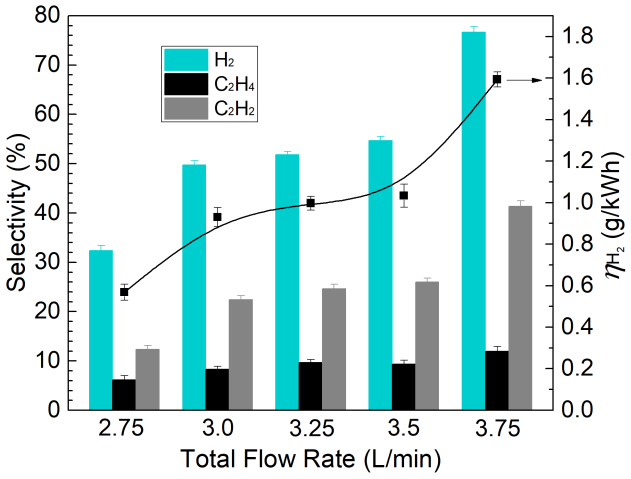

(b)

Figure 3. Influence of flow rate on (a) *n*-dodecane conversion, converted *n*-dodecane and energy efficiency; (b) the selectivity of major gas products and hydrogen production efficiency (*n*-dodecane concentration 935 ppm; plasma power 110 W).

Figure 3(b) presents the selectivity of the main gaseous products as a function of the total flow rate. Increasing the gas flow rate significantly enhanced the selectivity of hydrogen and hydrocarbons. The selectivity of C_2H_2 was enhanced by a factor of 3 from 12.3% to 41.4% when increasing the gas flow rate from 2.75 to 3.75 L/min; the

highest selectivity of H_2 (76.7%) and C_2H_4 (12.0%) were also achieved at the gas flow rate of 3.75 L/min. The change of the energy efficiency of hydrogen production with the gas flow rate showed the same tendency as the hydrogen selectivity, reaching its peak value of 1.59 g/kWh at 3.75 L/min. Interestingly, the selectivity of H_2 and C_2 hydrocarbons (C_2H_2 and C_2H_4) as a function of nitrogen flow rate followed the same evolution as the relative intensity of the N_2 second positive system (0, 0) band head at 337.1 nm, as shown in Figure S2 (Supporting Information). Note that the relative intensity of the N_2 second positive system (0, 0) band head is closely associated to the formation of excited nitrogen molecules, which suggests that increasing the nitrogen flow rate produces more excited N_2 species, resulting in the enhanced selectivity of hydrogen, C_2H_2 and C_2H_4. Similar phenomena were also reported in the degradation of hydrocarbons using gliding arc plasmas [36, 37]. These findings reveal that the gas flow rate is a key parameter affecting the generation of different gas products in this process and can be used to tune the selectivity of hydrogen and C_2 hydrocarbons. Higher gas flow is desirable to achieve higher energy efficiency, hydrogen production efficiency, and gas selectivity at the expense of slightly reduced conversion. In addition, we found that the distribution of these major gas products was closely correlated with the amount of converted *n*-dodecane and energy efficiency.

3.3 Influence of applied voltage

The applied voltage is a key plasma parameter used to control the power, which in turn affects the plasma chemical reactions. As seen in Figure S3, the discharge power

increased almost linearly and varied from 90 to 120 W when changing the applied voltage from 4.1 to 9.0 kV. Figure 4(a) plots the conversion of *n*-dodecane and energy efficiency as a function of applied voltage while keeping the *n*-dodecane concentration and total flow rate constant. Increasing the applied voltage enhanced the *n*-dodecane conversion from 62.4% to 77.1%, which can be attributed to the increased power input to the plasma reforming process. Note that the energy efficiency of this process remained stable at 9.5 g/kWh rather than declining when changing the applied voltage from 4.1 to 9.0 kV. This result provides valuable information for the scale-up of the process as the typical trade-off barrier between the efficiency and conversion can be overcome, i.e. higher conversion can be achieved at a higher power input without decreasing the energy efficiency.

Increasing the applied voltage also enhanced the selectivity of hydrogen and the energy efficiency of hydrogen production, as shown in Figure 4(b). The highest H_2 selectivity (57.8%) and hydrogen production efficiency (1.06 g/kWh) were obtained at an applied voltage of 9 kV. The enhanced process performance, including *n*-dodecane conversion, gas selectivity, and hydrogen production efficiency can be attributed to the elevated power input resulting in the generation of more electrons and reactive species for the chemical reactions. The increased frequency of effective collisions of these energetic species with *n*-dodecane and its intermediates contributed to their conversion [38]. Similarly, one significant advantage of this process is that

higher H_2 production efficiency and gas selectivity can be achieved without the compensation of reduced energy efficiency.

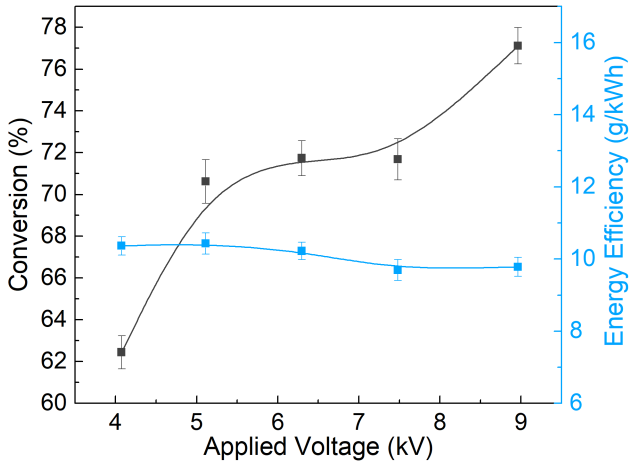

(a)

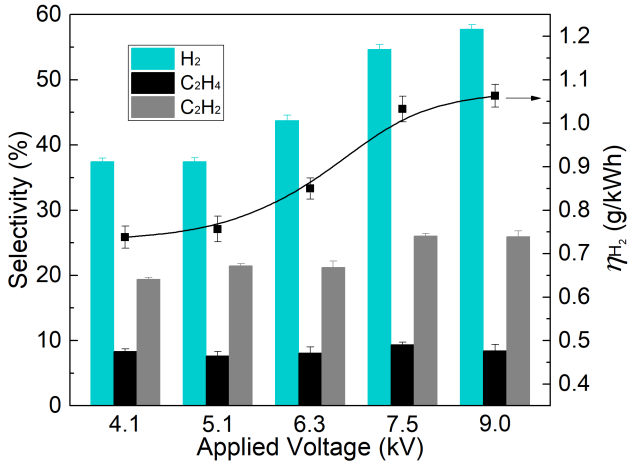

(b)

Figure 4. Influence of applied voltage on (a) *n*-dodecane conversion and efficiency; (b) the selectivity of major gas products and hydrogen production efficiency (*n*-dodecane concentration 935 ppm; total flow rate 3.5 L/min).

3.4 OES analysis of C_2 species

In addition to the gas analysis using GC, OES diagnostics were carried out to investigate the formation of C_2 species in the plasma conversion under different operating conditions. As seen in Figure 5, the generation of C_2 hydrocarbons can also be confirmed by the dominant C_2 Swan bands present in the plasma spectrum (Δv = -1, 0, +1 with the relevant band head at 472.0 nm, 516.7 nm, 563.5 nm, respectively) [39, 40].

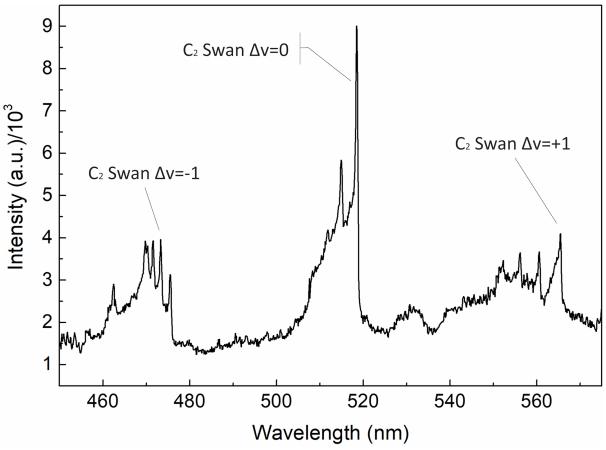

Figure 5. The optical emission spectrum of the N_2/*n*-$C_{12}H_{26}$/H_2O gliding arc plasma (spectral resolution 0.05 nm; grating 600 g/mm; exposure time 0.1 s; discharge power 110 W; *n*-dodecane concentration 935 ppm; total flow rate 3.5 L/min)

Figure 6 shows a linear relationship between the relative intensity of the C_2 band head at 516.7 nm and the total yield of C_2 hydrocarbons in the plasma reaction when changing either gas flow rate or applied voltage. The evolution of the C_2 yield with the total flow rate perfectly matches the change of the intensity of the C_2 band head (516.7 nm) as a function of nitrogen flow rate. These findings suggest that the emission bands of diatomic carbon C_2 can be used as a valuable probe to understand

the generation of C_2 hydrocarbons, especially C_2H_2 and C_2H_4, in the conversion of hydrocarbon oils.

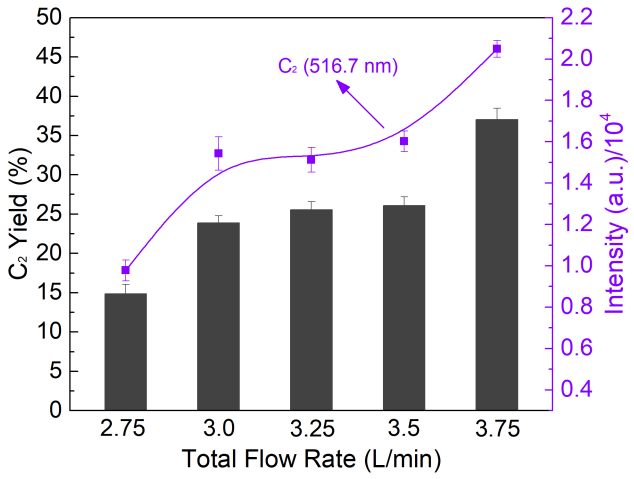

(a)

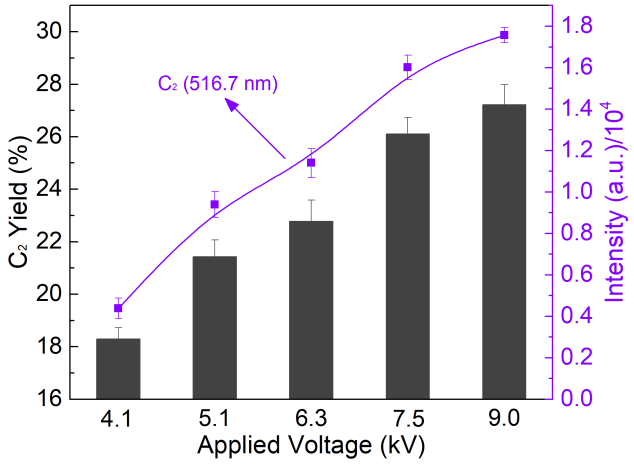

(b)

Figure 6. (a) Influence of total flow rate on the C_2 yield and relative intensity of the C_2 Swan band head (516.7 nm) at a constant discharge power of 110 W; (b) effect of applied voltage on the C_2 yield and relative intensity of the C_2 Swan band head (516.7 nm) at a constant total flow rate of 3.5 L/min. (*n*-dodecane concentration 935 ppm).

3.5 Comparison with other works

Table 1 compares the performance of different plasma systems for the conversion of heavy hydrocarbons conversion using different plasma systems. A high *n*-dodecane conversion of 68.1% and a high H_2 selectivity of 76.7% were achieved simultaneously using the GAD in this study. The selectivity of hydrogen obtained in this work is significantly higher than that achieved using DBD and thermal plasma. While the energy efficiency for hydrogen production using the GAD is comparable to that which has reported in previous literature, one should note that it is more energy consuming for the plasma cracking of *n*-dodecane when compared to light fuels (e.g. *n*-hexane). In addition, the use of nitrogen instead of argon as a carrier gas for the plasma cracking of hydrocarbon oils is more realistic from an industrial application standpoint due to the cost of argon. Our GAD plasma process has clearly shown significant advantages over other plasma processes for the conversion of hydrocarbon oils to hydrogen with high selectivity and production efficiency.

Table 1. A comparison of the performances of different plasma processes for the cracking of hydrocarbon oils.

Plasma type	Reactant	Carrier gas	Concn. [a] (g/m^3)	Flow rate (m^3/h)	*SEI* (kWh /m^3)	X [b] (%)	S_{H_2} [c] (%)	η_e [d] (g/kWh)	η_{H_2} [e] (g/kWh)	Ref.
Thermal plasma	*n*-hexane	Ar+H_2	304.2	0.7	5.5	90	12.2	54.1	2.2	[41]
DBD	*n*-heptane	Ar	268.4	0.01	0.8	35.1	8.5	108.2	1.5	[42]
DBD	*n*-decane	Ar	-	0.002	0.1	-	18.3	-	0.8	[43]
DBD	*n*-dodecane	N_2	0.5	0.1	0.01	21	-	9.5	-	[27]
GAD	*n*-dodecane	N_2	7.1	0.2	0.4	68.12	76.7	10.9	1.6	this work

[a] The abbreviation 'concn.' stands for the concentration of reactant.

[b] X stands for the conversion percentage of reactant fuels.

[c] S_{H_2} stands for the hydrogen selectivity.

[d] η_e stands for the energy efficiency of fuel conversion.

[e] η_{H_2} stands for the hydrogen production efficiency.

4. Reaction mechanism

Condensed liquid products collected in the plasma process were analyzed by GC-MS. Isomers of olefins from C_8 to C_{11} were identified as the dominant liquid chemicals including cyclopropane, pentyl- (C_8H_{16}); cyclopropane, 1-methyl-2-pentyl- (C_9H_{18}); 4-decene ($C_{10}H_{20}$); and 5-undecene ($C_{11}H_{22}$), as shown in Figure 7 and Scheme 1. One of the major liquid products (4-decene) was quantified with a selectivity of around 1.7%. Note that no cyanide products were detected even though nitrogen was used as the working gas. In this study, the distribution of these gasoline ranged fuels remained unchanged when changing the operating conditions, including *n*-dodecane concentration, total flow rate and applied voltage. Compared to the plasma aqueous reforming of *n*-dodecane in which versatile liquid products including heavier fuels (C_{13+}) and oxygenates were formed, this GAD-based plasma process produces mainly hydrogen, C_2 hydrocarbons and gasoline ranged fuels (C_8-C_{11}) without the formation of complicated by-products.

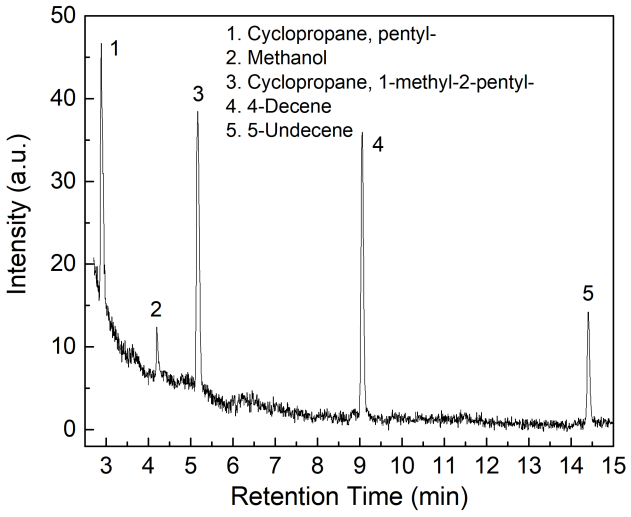

Figure 7. A typical GC-MS spectrum of the liquid chemicals formed in the plasma degradation of *n*-dodecane (discharge power 110 W; *n*-dodecane concentration 935 ppm; total flow rate 3.5 L/min).

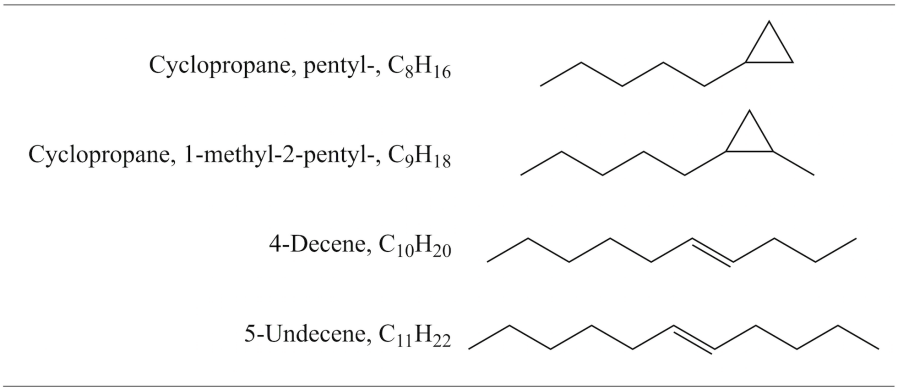

Scheme 1. Liquid products identified by GC-MS.

The decomposition of *n*-dodecane in the gliding arc can be initiated via H-abstraction of *n*-dodecane by electrons and excited nitrogen species to form dodecyl and hydrogen radicals (R1-R2). Excited nitrogen species play a far more dominant role when compared to energetic electrons, for the conversion of *n*-dodecane in this process, which has been supported by both experimental and modelling studies [44, 45]. Yu et al. demonstrated that nitrogen excited species contributed significantly to the decomposition of naphthalene with a low concentration in a GAD reactor, while electron impact dissociation made a minor contribution to the plasma degradation of $C_{10}H_8$ [46]. Aerts et al. developed a plasma chemical kinetic model to reveal the relative importance of active species (e.g. free radicals and nitrogen metastable species) in the plasma decomposition of ethylene. Their results showed that direct

dissociation of ethylene by electrons could be neglected, while the metastable nitrogen species dominates the destruction of ethylene [47].

$$n\text{-}C_{12}H_{26} + e \rightarrow C_{12}H_{25} + H + e \quad \text{(R1)}$$

$$n\text{-}C_{12}H_{26} + N_2^* \rightarrow C_{12}H_{25} + H + N_2 \quad \text{(R2)}$$

H-abstraction of *n*-dodecane by radicals such as H and CH_3 is also an important step for the dissociation of *n*-dodecane in the plasma process (R3-R4), while C-C fission was considered to play a minor role in the decomposition of *n*-dodecane due to a higher energy barrier [48, 49]. Jia et al. found that H-abstraction by the collisions of free radicals such as H and CH_3 contributed to more than 80% in the decomposition of a jet fuel surrogate [50].

$$n\text{-}C_{12}H_{26} + H \rightarrow C_{12}H_{25} + H_2 \quad \text{(R3)}$$

$$n\text{-}C_{12}H_{26} + CH_3 \rightarrow C_{12}H_{25} + CH_4 \quad \text{(R4)}$$

Previous studies on fuel pyrolysis found that the H-abstraction of *n*-$C_{12}H_{26}$ typically generates dodecyl radicals from 2-$C_{12}H_{25}$ to 6-$C_{12}H_{25}$ but not 1-$C_{12}H_{25}$ due to the presence of varying bond strengths at different positions of *n*-dodecane [51-54]. It is commonly accepted that BDEs differentiate the probability of single bond fissions, leading to different reaction rates. In this work, we have calculated the BDEs at different positions of *n*-dodecane to help elucidate the reaction pathway from the energetics of different C-H bonds. The comparison of the homolytic C-H BDEs computed using the B3LYP/6-311+G** level of theory is summarised in Table 1. The

BDE of the C-H bond at the α carbon of *n*-dodecane (4.62 eV) is clearly higher than that at other C sites (around 4.45 eV). As such, we believe that it is more difficult to form 1-$C_{12}H_{25}$, as H-abstraction of *n*-$C_{12}H_{26}$ to 1-$C_{12}H_{25}$ has a higher barrier and lower reaction rate compared to the relevant H-abstraction required for the formation of 2-$C_{12}H_{25}$ to 6-$C_{12}H_{25}$ radicals.

Table 1. Comparison of homolytic C-H BDEs in *n*-dodecane.

Reaction	BDE (eV)
n-$C_{12}H_{26} \rightarrow H + CH_3(CH_2)_{10}CH_2$	4.62
n-$C_{12}H_{26} \rightarrow H + CH_3(CH_2)_9CH \cdot CH_3$	4.46
n-$C_{12}H_{26} \rightarrow H + CH_3(CH_2)_8CH \cdot CH_2CH_3$	4.45
n-$C_{12}H_{26} \rightarrow H + CH_3(CH_2)_7CH \cdot (CH_2)_2CH_3$	4.45
n-$C_{12}H_{26} \rightarrow H + CH_3(CH_2)_6CH \cdot (CH_2)_3CH_3$	4.45
n-$C_{12}H_{26} \rightarrow H + CH_3(CH_2)_5CH \cdot (CH_2)_4CH_3$	4.45

The C-C bond cleavage of dodecyl radicals ($C_{12}H_{25}$) generates higher olefins, including C_8H_{16}, C_9H_{18}, $C_{10}H_{20}$, and $C_{11}H_{22}$, together with alkyl radicals (Scheme 1). In the β-C-C bond fission of dodecyl radicals, the transformation of $C_{12}H_{25}$ to other types of isomer could occur through mutual isomerization reactions [55]. The isomerization happens during the cracking of several long-chain *n*-alkanes [56, 57]. Figure 8 summarizes a typical mutual isomerization mechanism in the plasma conversion of *n*-dodecane. Similar mutual isomerizations of lower alkyl radicals could

also take place in this process, as evidenced by the alternation of intermediates (1-alkenes) to final liquid products (see Scheme 1) [49, 58].

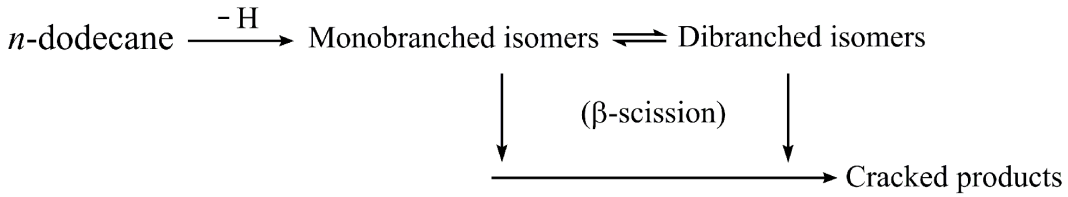

Figure 8. Scheme of mutual isomerization in *n*-dodecane cracking.

The liquid products cyclopropane, pentyl- (C_8H_{16}) and cyclopropane, 1-methyl-2-pentyl- (C_9H_{18}) could be produced via the formation of cyclopropane [59]. As shown in R5, alkenes can react with the abundant, highly activated methylene species to form cyclopropane.

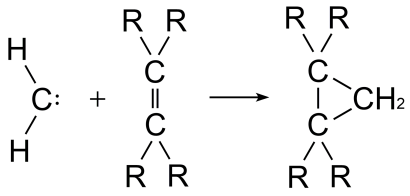

(R5)

H-abstractions and β-scissions of higher alkene and alkyl intermediates (e.g. C_8-C_{11}) form lower hydrocarbons, which then subsequently undergo cracking or recombination to produce the final gaseous products. The possible reactions for the dissociation and formation of lower hydrocarbons in the GAD cracking of *n*-dodecane are summarized in R6-R13. The decomposition of C_4H_9 forms C_2H_5 and ethylene (R6) and is followed by subsequent H-abstraction reactions shown in R9 and R10. The H-abstraction of C_3H_7 followed by the C-C bond dissociation of C_3H_6 forms methane

and acetylene. Other plausible reaction routes for acetylene formation are shown in R10-R12. The generation of carbon deposition could be associated with the decomposition of C_2H_2 (R13) [60].

$$C_4H_9 \rightarrow C_2H_5 + C_2H_4 \quad \text{(R6)}$$

$$C_3H_7 \rightarrow C_3H_6 + H \quad \text{(R7)}$$

$$C_3H_6 \rightarrow C_2H_2 + CH_4 \quad \text{(R8)}$$

$$C_2H_5 \rightarrow C_2H_4 + H \quad \text{(R9)}$$

$$C_2H_4 \rightarrow C_2H_3 + H \quad \text{(R10)}$$

$$C_2H_3 \rightarrow C_2H_2 + H \quad \text{(R11)}$$

$$C_2H_4 \rightarrow C_2H_2 + H_2 \quad \text{(R12)}$$

$$C_2H_2 \rightarrow 2C + H_2 \quad \text{(R13)}$$

Figure 9 shows the proposed plausible reaction pathways in the GAD-assisted conversion of *n*-dodecane, based on a comprehensive analysis of the gas and liquid products coupled with OES diagnostics from this work alongside the simulation results from the previous literature. In summary, the degradation of *n*-dodecane in the GAD can proceed through the following steps: (1) initial dehydrogenation of *n*-$C_{12}H_{26}$ by electrons and nitrogen excited species; (2) secondary H-abstraction of *n*-$C_{12}H_{26}$ by radicals such as H atoms; (3) mutual isomerization of alkyl radicals ($C_{12}H_{25}$); (4) β-scission of alkyl to generate alkenes and lower alkyl species; (5) H-abstraction of alkenes; (6) decomposition of alkenyl species.

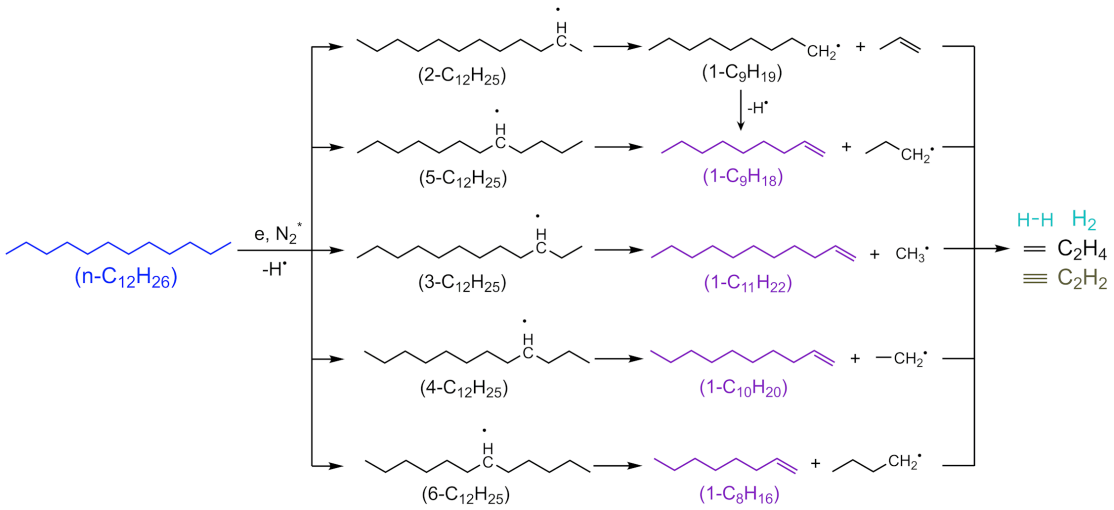

Figure 9. Proposed reaction pathways of the plasma degradation of *n*-dodecane.

5. Conclusion

In this study, a knife-shaped gliding arc reactor has been developed for the co-generation of CO_x-free hydrogen and C_2 hydrocarbons (C_2H_2 and C_2H_4) via *n*-dodecane cracking at low temperatures. In addition to the production of hydrogen, this process also formed ethylene and acetylene with high selectivity as well as liquid gasoline ranged fuels. The conversion of *n*-dodecane, the selectivity of major gas products and the energy efficiency can be tuned by controlling the process parameters including *n*-dodecane concentration, total flow rate and applied voltage. The highest selectivity of H_2, C_2H_2, and C_2H_4 reached 76.7%, 41.4%, and 12.0%, respectively, at an input power of 110 W and with an *n*-dodecane conversion of 68.1%. The production of a CO_x-free hydrogen-rich gas mixture makes this process attractive for the further synthesis of olefins (an industrially important chemical feedstock), via the in-situ hydrogenation of acetylene. In addition, we found that higher conversion of

n-dodecane and gas selectivity can be achieved when increasing power input without reducing the energy efficiency of the process. The OES diagnostics of the GAD showed that the relative intensity of the C_2 Swan bands is strongly correlated to the production of C_2 hydrocarbons in the plasma reforming of *n*-dodecane. The dissociation of *n*-dodecane is believed to be dominated by the H-abstraction via nitrogen excited species N_2^* and radicals (e.g. H and CH_3). The mutual isomerization of alkyl radicals ($C_{12}H_{25}$) took place followed by subsequent β-scission and H-abstraction to generate alkenes and lower alkyl radicals. The gasoline range liquid chemicals were formed via the reaction route of cyclopropane formation.

Acknowledgement

The support of this work by the UK EPSRC Impact Acceleration Account (IAA) is gratefully acknowledged. Y. Ma acknowledges the PhD fellowship co-funded by the University of Liverpool and the Chinese Scholarship Council (CSC).

Reference

[1] Vita A, Italiano C, Fabiano C, Pino L, Laganà M, Recupero V. Hydrogen-rich gas production by steam reforming of n -dodecane. Applied Catalysis B: Environmental 2016;199:350-60.

[2] Kim S, Sasmaz E, Lauterbach J. Effect of Pt and Gd on coke formation and regeneration during JP-8 cracking over ZSM-5 catalysts. Applied Catalysis B: Environmental 2015;168-169:212-9.

[3] Li L, Shang Z, Xiao Z, Wang L, Liang X, Liu G. Steam reforming of n-dodecane over mesoporous alumina supported nickel catalysts: Effects of metal-support interaction on nickel catalysts. International Journal of

Hydrogen Energy 2019;44(13):6965-77.
[4] Lo Faro M, Trocino S, Zignani SC, Italiano C, Vita A, Aricò AS. Study of a solid oxide fuel cell fed with n-dodecane reformate. Part II: Effect of the reformate composition. International Journal of Hydrogen Energy 2017;42(3):1751-7.
[5] Fabiano C, Italiano C, Vita A, Pino L, Laganà M, Recupero V. Performance of 1.5 Nm3/h hydrogen generator by steam reforming of n-dodecane for naval applications. International Journal of Hydrogen Energy 2016;41(42):19475-83.
[6] Lo Faro M, Trocino S, Zignani SC, Aricò AS, Maggio G, Italiano C, et al. Study of a Solid Oxide Fuel Cell fed with n-dodecane reformate. Part I: Endurance test. International Journal of Hydrogen Energy 2016;41(13):5741-7.
[7] Navarro RM, Pena MA, Fierro JL. Hydrogen production reactions from carbon feedstocks: fossil fuels and biomass. Chem Rev 2007;107(10):3952-91.
[8] Dincer I, Acar C. Review and evaluation of hydrogen production methods for better sustainability. International Journal of Hydrogen Energy 2015;40(34):11094-111.
[9] Andrews J, Shabani B. Re-envisioning the role of hydrogen in a sustainable energy economy. International Journal of Hydrogen Energy 2012;37(2):1184-203.
[10] Ji S, Xiao Z, Zhang H, Li L, Li G, Wang L, et al. Catalytic steam reforming of n-dodecane over high surface area Ce0.75Zr0.25O2 supported Ru catalysts. International Journal of Hydrogen Energy 2017;42(49):29484-97.
[11] Rahimi N, Karimzadeh R. Catalytic cracking of hydrocarbons over modified ZSM-5 zeolites to produce light olefins: A review. Applied Catalysis A: General 2011;398(1-2):1-17.
[12] Yaripour F, Shariatinia Z, Sahebdelfar S, Irandoukht A. Conventional hydrothermal synthesis of nanostructured H-ZSM-5 catalysts using various templates for light olefins production from methanol. Journal of Natural Gas Science and Engineering 2015;22:260-9.
[13] Kirilin AV, Dewilde JF, Santos V, Chojecki A, Scieranka K, Malek A. Conversion of Synthesis Gas to Light Olefins: Impact of Hydrogenation Activity of Methanol Synthesis Catalyst on the Hybrid Process Selectivity over Cr–Zn and Cu–Zn with SAPO-34. Industrial & Engineering Chemistry Research 2017;56(45):13392-401.
[14] Sadrameli SM. Thermal/catalytic cracking of liquid hydrocarbons for the production of olefins: A state-of-the-art review II: Catalytic cracking review. Fuel 2016;173:285-97.
[15] Moulijn JA, Van Diepen A, Kapteijn F. Catalyst deactivation: is it predictable?: What to do? Applied Catalysis A: General 2001;212(1-2):3-16.
[16] Xiao Z, Wu C, Li L, Li G, Liu G, Wang L. Pursuing complete and stable steam reforming of n-dodecane over nickel catalysts at low temperature and high LHSV. International Journal of Hydrogen Energy 2017;42(8):5606-18.

[17] Fridman A. Plasma Chemistry. Cambridge: Cambridge University Press; 2008.
[18] Mei D, Tu X. Conversion of CO2 in a cylindrical dielectric barrier discharge reactor: Effects of plasma processing parameters and reactor design. Journal of CO2 Utilization 2017;19:68-78.
[19] Wang L, Yi Y, Guo H, Tu X. Atmospheric Pressure and Room Temperature Synthesis of Methanol through Plasma-Catalytic Hydrogenation of CO2. ACS Catalysis 2018;8(1):90-100.
[20] Kalra CS, Gutsol AF, Fridman AA. Gliding arc discharges as a source of intermediate plasma for methane partial oxidation. IEEE Transactions on Plasma Science 2005;33(1):32-41.
[21] Fridman A, Gutsol A, Gangoli S, Ju Y, Ombrello T. Characteristics of Gliding Arc and Its Application in Combustion Enhancement. Journal of Propulsion and Power 2008;24(6):1216-28.
[22] Zhang H, Zhu F, Li X, Xu R, Li L, Yan J, et al. Steam reforming of toluene and naphthalene as tar surrogate in a gliding arc discharge reactor. Journal of Hazardous Materials 2019;369:244-53.
[23] Wang L, Liu S, Xu C, Tu X. Direct conversion of methanol to n-C 4 H 10 and H 2 in a dielectric barrier discharge reactor. Green Chemistry 2016;18(20):5658-66.
[24] Zhang H, Li X, Zhu F, Cen K, Du C, Tu X. Plasma assisted dry reforming of methanol for clean syngas production and high-efficiency CO2 conversion. Chemical Engineering Journal 2017;310:114-9.
[25] Zhu F, Zhang H, Yan X, Yan J, Ni M, Li X, et al. Plasma-catalytic reforming of CO 2 -rich biogas over Ni/γ-Al 2 O 3 catalysts in a rotating gliding arc reactor. Fuel 2017;199:430-7.
[26] Zhang H, Wang W, Li X, Han L, Yan M, Zhong Y, et al. Plasma activation of methane for hydrogen production in a N2 rotating gliding arc warm plasma: A chemical kinetics study. Chemical Engineering Journal 2018;345:67-78.
[27] Prantsidou M, Whitehead JC. The Chemistry of Gaseous Dodecane Degradation in a BaTiO3 Packed-Bed Plasma Reactor. Plasma Chemistry and Plasma Processing 2014;35(1):159-72.
[28] Whitehead JC, Prantsidou M. Investigation of hydrocarbon oil transformation by gliding arc discharge: comparison of batch and recirculated configurations. Journal of Physics D: Applied Physics 2016;49(15):154001.
[29] Zhang X, Cha MS. Tailored reforming of n-dodecane in an aqueous discharge reactor. Journal of Physics D: Applied Physics 2016;49(17):175201.
[30] Piavis W, Turn S, Ali Mousavi SM. Non-thermal gliding-arc plasma reforming of dodecane and hydroprocessed renewable diesel. International Journal of Hydrogen Energy 2015;40(39):13295-305.
[31] Matsui Y, Kawakami S, Takashima K, Katsura S, Mizuno A. Liquid-phase fuel re-forming at room temperature using nonthermal plasma. Energy & fuels 2005;19(4):1561-5.
[32] Jahanmiri A, Rahimpour MR, Mohamadzadeh Shirazi M, Hooshmand N, Taghvaei H. Naphtha cracking through a pulsed DBD plasma reactor: Effect

of applied voltage, pulse repetition frequency and electrode material. Chemical Engineering Journal 2012;191:416-25.
[33] Gallagher MJ, Geiger R, Polevich A, Rabinovich A, Gutsol A, Fridman A. On-board plasma-assisted conversion of heavy hydrocarbons into synthesis gas. Fuel 2010;89(6):1187-92.
[34] Ray D, Manoj Kumar Reddy P, Challapalli S. Glass Beads Packed DBD-Plasma Assisted Dry Reforming of Methane. Topics in Catalysis 2017;60(12):869-78.
[35] Tu X, Whitehead JC. Plasma-catalytic dry reforming of methane in an atmospheric dielectric barrier discharge: Understanding the synergistic effect at low temperature. Applied Catalysis B: Environmental 2012;125:439-48.
[36] Chun YN, Kim SC, Yoshikawa K. Destruction of anthracene using a gliding arc plasma reformer. Korean Journal of Chemical Engineering 2011;28(8):1713.
[37] Tu X, Whitehead JC. Plasma dry reforming of methane in an atmospheric pressure AC gliding arc discharge: Co-generation of syngas and carbon nanomaterials. International Journal of Hydrogen Energy 2014;39(18):9658-69.
[38] Liu S, Mei D, Wang L, Tu X. Steam reforming of toluene as biomass tar model compound in a gliding arc discharge reactor. Chemical Engineering Journal 2017;307:793-802.
[39] Riascos H, Zambrano G, Prieto P. Spectroscopic Analysis of a Pulsed-Laser Deposition System for Fullerene-like Cn x Film Production. Plasma Chemistry and Plasma Processing 2006;26(3):277-91.
[40] Wang L, Yi Y, Wu C, Guo H, Tu X. One-Step Reforming of CO2 and CH4 into High-Value Liquid Chemicals and Fuels at Room Temperature by Plasma-Driven Catalysis. Angew Chem Int Ed Engl 2017;56(44):13679-83.
[41] Yan B, Xu P, Li X, Guo CY, Jin Y, Cheng Y. Experimental Study of Liquid Hydrocarbons Pyrolysis to Acetylene in H2/Ar Plasma. Plasma Chemistry and Plasma Processing 2012;32(6):1203-14.
[42] Manoj Kumar Reddy P, Cha MS. Selective control of reformed composition of n-heptane via plasma chemistry. Fuel 2016;186:150-6.
[43] Song F, Wu Y, Xu S, Jin D, Jia M. N-decane decomposition by microsecond pulsed DBD plasma in a flow reactor. International Journal of Hydrogen Energy 2019;44(7):3569-79.
[44] Guerra V, Sa P, Loureiro J. Role played by the N2 (A3Σu+) metastable in stationary N2 and N2-O2 discharges. Journal of Physics D: Applied Physics 2001;34(12):1745.
[45] Herron JT. Evaluated Chemical Kinetics Data for Reactions of N(2D), N(2P), and N2(A3Σu+) in the Gas Phase. Journal of Physical and Chemical Reference Data 1999;28(5):1453-83.
[46] Yu L, Li X, Tu X, Wang Y, Lu S, Yan J. Decomposition of Naphthalene by dc Gliding Arc Gas Discharge. The Journal of Physical Chemistry A 2010;114(1):360-8.

[47] Aerts R, Tu X, De Bie C, Whitehead JC, Bogaerts A. An Investigation into the Dominant Reactions for Ethylene Destruction in Non‐Thermal Atmospheric Plasmas. Plasma Processes and Polymers 2012;9(10):994-1000.
[48] You X, Egolfopoulos FN, Wang H. Detailed and simplified kinetic models of n-dodecane oxidation: The role of fuel cracking in aliphatic hydrocarbon combustion. Proceedings of the Combustion Institute 2009;32(1):403-10.
[49] Zeng M, Yuan W, Wang Y, Zhou W, Zhang L, Qi F, et al. Experimental and kinetic modeling study of pyrolysis and oxidation of n-decane. Combustion and Flame 2014;161(7):1701-15.
[50] Jia Z, Wang Z, Cheng Z, Zhou W. Experimental and modeling study on pyrolysis of n-decane initiated by nitromethane. Combustion and Flame 2016;165:246-58.
[51] Zhao L, Yang T, Kaiser RI, Troy TP, Ahmed M, Ribeiro JM, et al. Combined Experimental and Computational Study on the Unimolecular Decomposition of JP-8 Jet Fuel Surrogates. II: n-Dodecane (n-C12H26). J Phys Chem A 2017;121(6):1281-97.
[52] Sivaramakrishnan R, Michael JV, Ruscic B. High-temperature rate constants for H/D + C2H6 and C3H8. International Journal of Chemical Kinetics 2012;44(3):194-205.
[53] Wang Q-D, Wang J-B, Li J-Q, Tan N-X, Li X-Y. Reactive molecular dynamics simulation and chemical kinetic modeling of pyrolysis and combustion of n-dodecane. Combustion and Flame 2011;158(2):217-26.
[54] Zhao L, Yang T, Kaiser RI, Troy TP, Ahmed M, Belisario-Lara D, et al. Combined Experimental and Computational Study on the Unimolecular Decomposition of JP-8 Jet Fuel Surrogates. I. n-Decane (n-C10H22). J Phys Chem A 2017;121(6):1261-80.
[55] Kissin YV. Chemical mechanisms of catalytic cracking over solid acidic catalysts: Alkanes and alkenes. Catal Rev 2001;43(1-2):85-146.
[56] Martens JA, Jacobs PA, Weitkamp J. Attempts to Rationalize the Distribution of Hydrocracked Products. I Qualitative Description of the Primary Hydrocracking Modes of Long Chain Paraffins in Open Zeolites. Applied Catalysis 1986;20:239-81.
[57] Jacobs PA, Martens JA, Weitkamp J, Beyer HK. Shape-selectivity changes in high-silica zeolites. Faraday Discussions of the Chemical Society 1981;72:353.
[58] Banerjee S, Tangko R, Sheen DA, Wang H, Bowman CT. An experimental and kinetic modeling study of n -dodecane pyrolysis and oxidation. Combustion and Flame 2016;163:12-30.
[59] McMurry J. Organic chemistry 7th Edition. Belmont, USA: Thomson Brooks/Cole; 2008.
[60] Raseev S. Thermal and catalytic processes in petroleum refining. New York, USA: CRC Press; 2003.